On-line monitoring of solar cell module production by ellipsometry technique

M. Fried

PII: S0040-6090(14)00350-2
DOI: doi: 10.1016/j.tsf.2014.03.058
Reference: TSF 33310

To appear in: *Thin Solid Films*

Received date: 24 June 2013
Revised date: 15 March 2014
Accepted date: 16 March 2014

Please cite this article as: M. Fried, On-line monitoring of solar cell module production by ellipsometry technique, *Thin Solid Films* (2014), doi: 10.1016/j.tsf.2014.03.058

On-line monitoring of solar cell module production by ellipsometry technique

M. Fried[1, 2]

[1]*Institute for Technical Physics and Materials Science, Research Centre for Natural Sciences (MTA TTK MFA), H-1525 Budapest, POB 49, Hungary*

[2]*Doctoral School of Molecular – and Nanotechnologies, Faculty of Information Technology, University of Pannonia, Egyetem u. 10, Veszprém, H-8200, Hungary*

Abstract

Non-destructive analysing tools are needed at all stages of thin film photovoltaic (PV) development, and on production lines. In thin film PV, layer thicknesses, micro-structure, composition, layer optical properties, and their uniformity (because each elementary cell is connected electrically in series within a big panel) serve as an important starting point in the evaluation of the performance of the cell or module. An important focus is to express the dielectric functions of each component material in terms of a handful of wavelength independent parameters whose variation can cover all process variants of that material. With the resulting database, spectroscopic ellipsometry coupled with multilayer analysis can be developed for on-line point-by-point mapping and on-line line-by-line imaging.

This work tries to review the investigations of different types of PV-layers (anti-reflective coating, transparent-conductive oxide (TCO), multi-diode-structure, absorber and window layers) showing the existing dielectric function databases for the thin film components of CdTe, $CuInGaSe_2$, thin Si, and TCO layers.

Off-line point-by-point mapping can be effective for characterization of non-uniformities in full scale PV panels in developing labs but it is slow in the on-line mode when only 15 points can be obtained (within 1 min) as a 120 cm long panel moves by the mapping station. In the last years [M. Fried et al., *Thin Solid Films* **519**, 2730 (2011)], instrumentation was developed that provides a line image of spectroscopic ellipsometry (wl=350-1000 nm) data. Upto now a single 30 point line image can be collected in 10 s over a 15 cm width of PV material. This year we are building a 30 and a 60 cm width expanded beam ellipsometer the speed of which will be increased by 10X. Then 1800 points can be mapped in a 1 min traverse of a 60*120 cm PV panel or flexible roll-to-roll substrate.

e-mail: fried@mfa.kfki.hu

Introduction and trends in PhotoVoltaic Industry

Production and installation of PhotoVoltaic (PV) modules grew exponentially in the last decade. The thin film PV production and installation has grown similarly, or even faster, because its market share has grown from 5 % upto 15 %. Presently, CdTe and $CuInGaSe_2$ (CIGS) based thin film PV-s are overgrown the a-Si type PV-s. The best and average efficiences of all types of PV-modules are growing continuosly. At the same time, the relative fabrication cost (i.e. price of $Watt_{peak}$) and energy pay-back time continuosly reducing and one can see from the so called "price learning curves" that the different thin film technologies are well ahead in cost effectiveness against the bulk crystalline Si-technologies. [Photovoltaics Report (Roland Schindler (Fraunhofer ISE) and Werner Warmuth (PSE AG)), Freiburg, December 11, 2012, www.ise.fraunhofer.de, Fraunhofer Institute for Solar Energy System ISE]

Longitudinal elementary cells are connected electrically in series in thin film solar panels and the module power is limited by the elementary cell with the lowest current, so structural uniformity is essential to achieve high efficiency. If we want to close the gap between „Lab cell" and „Industrial module" efficiency, the key factor to increase the efficiency in the case of thin-film solar panels or modules is the lateral homogeneity.

What can we measure on PhotoVoltaic structures by Spectroscopic Ellipsometry (SE)?

The last decades have seen widespread use of SE in different fields of research. Ellipsometry offers great promise for characterization, monitoring, and control of a wide variety of processes, especially in semiconductor related areas [1-12]

Micromorph silicon solar cell structures

An understanding of the relationship between materials property and thin-film solar cell performance variations over large areas is of interest for evaluating the impact of macroscopic non-uniformities in scale-up from laboratory cells to production modules. One can spatially correlate the properties of the hydrogenated silicon (a-Si:H) i- and p-layers—as mapped over a larger substrate area—with device performance parameters from an array of a-Si:H based n-i-p dot cells. Analysis of the SE data over the full area provides maps of i-layer thickness and band gap, p-layer thickness and band gap, and p-layer surface roughness thickness for the n-i-p solar cell structure. The mapped values adjacent to the devices can be correlated with photovoltaic (PV) device performance parameters. When sufficient nonuniformity exists, these correlations enable optimization based on specific values of the fundamental properties. Alternatively, if the optimum set of properties has been identified, the impact of deviations due to macroscopic uniformities can be evaluated. [13]

CIGS solar cell structures

In the case of CIGS ($Cu(In_{1-x}Ga_x)Se_2$) the compositional change is an additional parameter. SE has the potential to map the alloy composition of CIGS thin films. This technique not only generates a compositional map but simultaneously provides maps of the more typical SE-determined properties as well, including bulk layer and surface roughness layer thicknesses. As a result, the methodology is suitable for characterization in online production-level applications. In order to develop the mapping capability, CIGS films having different molar Ga contents x and fixed copper stoichiometry were deposited and measured in situ by SE in order to extract the complex dielectric functions ($\varepsilon = \varepsilon_1 + i\varepsilon_2$) of these films. [14] For mathematical interpolation between the available alloy contents, the (ε_1, ε_2) spectra were parameterized using an oscillator sum. Best-fitting equations were obtained that relate each oscillator parameter to the Ga content x, as determined by energy dispersive X-ray analysis. This approach reduces the number of fitting parameters for (ε_1, ε_2) from several to just one: the Ga content x. [15-18] Because (ε_1, ε_2) is now represented by this single parameter, the chances of parameter correlations during fitting are reduced, enabling production-scale compositional mapping of chalcopyrite films by SE.

Broadening of optical transitions in polycrystalline CdS and CdTe thin films

The dielectric functions of polycrystalline CdS and CdTe thin films can be measured by in situ SE. Differences in due to processing variations are well understood using an excited carrier scattering model. A carrier mean free path can be defined that is found to be inversely proportional to the broadening of each of the band structure critical points (CPs). With this database, dielectric functions can be analyzed to evaluate the quality of materials used in CdS/CdTe photovoltaic heterojunctions. [19, 20]

Transparent Conductive Oxides (TCO)

Using appropriate optical models, the characterization of the layer thickness and carrier properties becomes possible from SE analysis, even for textured surfaces.

SE analysis of textured SnO_2:F substrate

The dielectric functions of the bulk SnO_2:F layers are well represented using a Tauc–Lorentz oscillator term to describe the interband transitions and a Drude term to describe the free electrons. [21, 22] In order to express the complicated optical response in the textured structures, the optical model can incorporate (i) the surface roughness and interface layers calculated using an effective-medium-approximation multilayer model and (ii) the a-Si:H/SnO2:F structure divided into two regions with different thicknesses. [23]

SE analysis of ZnO:Al

SE measurements can be used to measure the dielectric function of the ZnO:Al films. Monitoring of the electrical properties of Al-doped ZnO layers by SE measurements are feasible by using the analytical expression suggested by Yoshikawa and Adachi [24], and the results show correlation between specific resistance and band gap energy and direct exciton strength parameter. [25]

Characterization of SiH_2 content in a-Si:H

For hydrogenated amorphous silicon (a-Si:H) layers prepared by plasma-enhanced chemical vapor deposition, SiH_2 bonds exist at the internal surface of the void-rich structure and light absorption reduces due to the void formation. In particular, the amplitude of the ε_2 spectra obtained from various a-Si:H layers is expressed completely by the SiH_2 bond density in the a-Si:H and reduces strongly with increasing the SiH_2 content, indicating that microvoids present in the a-Si:H network are surrounded by the SiH_2 bonding state. Validity of SiH_2 analysis can be confirmed from IR ellipsometry. [26]

One remark

We must note that there are not enough raw materials (Cd, Te, In, Se) for the best (CdTe, CIGS) thin film PV technologies if one think in TeraWatt scale! There is an urgent need to research after new (High Concentration (concentration factor 300-1000 suns) Photovoltaic Systems i.e. III-V multi-Junction tandem cells or high multiple exciton generation nanoparticles with tunable optical gaps) or cheaper thin film technologies such as the $Cu_2ZnSn(S,Se)_4$ (CZTS) quaternary semiconductor compound which has similar properties as CdTe and CIGS! [27-37]

Fast SE-mapping by expanded beam ellipsometry

The highest efficiencies measured on laboratory-sized thin film solar cells are generally well ahead of the best production module efficiencies. Thus, in photovoltaic (PV) production for commercialization many key problems are related to scale-up. The difference is primarily caused by fluctuations in area uniformity of properties caused by the individual processing steps. The primary problem with many mapping probes [e.g., single-spot spectroscopic ellipsometry (SE), Kelvin probe, laser beam induced currents, etc.] is their reduced utility due to the long measurement time that makes in-line mapping impossible. We developed and (in this work) we demonstrate a high-speed and high-resolution measurement method to monitor the thin film PV process in-line over large areas.

Ellipsometry determines angle-of-incidence dependent relative amplitude ratios and phase difference shifts upon specular reflection of light from a planar surface. Thus, collimated light beams are conventionally used with a well defined angle of incidence at the reflecting surface. Here we present an ellipsometric method fundamentally different from the conventional techniques [38-42]. In our instrument, the sample is illuminated by an almost diffuse, "divergent beam" of light, providing a collection of rays with diverse angles of incidence at every point of the sample. Precise "angle-selection" is performed on the detector side by a pin-hole camera. The pin-hole works as an "angle-of-incidence filter", selecting only one single light-beam from every direction (or sample position). The angular resolution of this type of camera is dependent on the diameter of the pin-hole. In the case of a single wavelength measurement, this instrument solution is appropriate for measuring a large area sample with possible non-uniform properties such that the pinhole camera selects a single angle of incidence corresponding to each sample point, but that angle varies across the sample. If the sample is moved parallel to its surface along a line during the measurement, however, each sample point will experience multiple angles of incidence successively, which provides additional information to assist in data analysis. By repeating the measurement with light of various wavelengths, multi-angle, multi-wavelength (but not continuous spectroscopic) ellipsometry data can be acquired; see ref. [39, 40].

By confining the number of measured sample points to a narrow range along a line only, we can generate continuous spectroscopic data at each point along the line image using white light illumination with a spectral dispersion (grating) after the pin-hole. This instrument produces spatial information in one dimension of the CCD array simultaneously with spectroscopic information in the perpendicular direction of the array; see Fig. 1. Both ellipsometric approaches (multi-angle/multi-wavelength and continuous spectroscopic) are useful, for example, in the analysis of product moving along a coating line.

Instrumentation

A near-ultraviolet-to-visible (nuv-vis) range (350 - 630 nm) of the first generation divergent beam instrument [41, 42] were built in MFA, Budapest, but this prototype limits potential photovoltaics applications; as a result, an extension into the near-infrared (NIR) region were performed to probe below the band gap of absorber layers in order to measure their thicknesses (Fig. 2). Thus, with a broadened spectral range, it became possible to characterize a wider variety of layers and structures. Divergent beam ellipsometers (using uncollimated beam) employ film polarizers, which exhibit a wide semi-field angle but limited spectral range. In earlier state, dual spectral range capability was a convenient solution whereby the optical elements (source, polarizer-analyzer pairs, and optical grating) were automatically interchangeable, and the entire nuv-nir (350-1000 nm) spectra for a line image was detectable in two measurement cycles with one CCD camera [42], see Fig. 2.

Calibrations of the angle of incidence (relationship of pixel number to angle) and the mirror effects are performed via well-known and optimized structures, in this case three SiO_2/Si samples with different thicknesses. Although the precision and accuracy of the instrument is not higher than that of standard step-wise wavelength scanning ellipsometers that probe a single spot, it is capable of determining the thickness of a silicon-dioxide film with sub-nanometer precision and the angle-of-incidence with sub-tenth-degree precision in the calibration process. Mirror and possible window effects are calculated using the following equation:

$$\rho_{opt}=\rho_{meas}*\rho_{mirror}$$ (*different for each point and each wavelength*) [eq. 1]

where ρ_{opt} is the measured value without mirrors and windows, ρ_{meas} is the actually measured value, and ρ_{mirror} is the effect of the mirrors and the windows of the chamber (if any). The actual values of ρ_{mirror} are theoretically different for each sample position and each wavelength; however, these dependences are relatively weak. By

calibrating with three SiO_2/Si samples having different thicknesses, 3N (ψ, Δ) values are measured for each sample position (where N is the number of wavelengths), and 2N+4 unknown values must be determined by fitting for a full calibration. These include N pairs of {Re(ρ_{mirror}), Im(ρ_{mirror})}, along with three thicknesses and one angle of incidence. The calibration can be performed independently for each pixel of the CCD; however, improved signal-to-noise is obtained by summing the irradiances according to pixel-groups, in consideration of the lateral resolution of the system. After an initial attempt, the calibration values are smoothed as a function of sample position and wavelength using second order polynomials. A smooth variation is expected for the angle of incidence and for the {Re(ρ_{mirror}), Im(ρ_{mirror})} values. As a result, smoothing of the dependence of angle of incidence on position as well as the dependence of ρ_{mirror} on position and wavelength reduces errors in the calibration measurement [42].

Rotating compensator multi channel mapping ellipsometry

Rotating polarizer or analyzer measuring mode is not the optimal (especially when tan ψ is high and/or cos Δ is close to 1 or -1. We have investigated the performance gain of rotating compensator multi channel mapping ellipsometry, too!

We used an air spaced zero-order MgF_2 quarter wave retarder after the polarizer (from Karl Lambrecht Co.) with an equivalent rotating mechanism as is used with the analyzer and polarizer. After careful calibration (most part of the beam is going through at non-normal direction through the compensator) we have the angle of incidences, the mirror-(window)-corrections and the δ-shift by the retarder at all sample(-CCD)-points.

Demonstration sample preparations

Thermal oxide layers on 6-inch Si-wafers were prepared in usual furnace for calibrating and validating measurements. Poly-Si layer on SiO_2 on 6-inch Si-wafer (poly-Si 46) were prepared by LPCVD.

ZnO layer were deposited by magnetron sputtering onto Ag-covered plastic foil in a cassette roll-to-roll model machine.

Hydrogenated amorphous silicon (a-Si:H), nanocrystalline silicon (nc-Si:H), and mixed phase layers were deposited by very high frequency plasma enhanced chemical vapor deposition (vhf PECVD) onto ~ 15 x 15 cm^2 soda lime glass (SLG) and ~ 5 x 5 cm^2 Si wafer substrates. A thin Cr layer was sputtered onto the SLG prior the Si:H layer deposition to ensure adhesion and form a standard reflective interface for further SE measurement. The 5 x 30 cm^2 Cr target was located at a distance of 7 cm from the substrate. The sputtering in all cases was performed for 40 minutes with 0.67 Pa Ar gas and at 40 W rf power. The parallel depositions on 5 cm Si wafer substrates were carried out with the same parameters in order to study the layers by cross sectional transmission electron microscopy (XTEM).

The deposition conditions for the Si:H films studied here are summarized in Table 1. The vhf PECVD electrode size is approximately 15 x 15 cm^2, and the applied vhf frequency was 70 MHz. Prior to deposition all substrates were preheated to a temperate of 200 °C. The measured samples were deposited as part of an ongoing program for tandem a-Si:H/nc-Si:H silicon solar cell development. In the case of these solar materials, analyses of the processes for phase evolution and uniformity are crucial. XTEM images are shown for two such films in Fig. 6. The film prepared with R=20 (left) evolves from a-Si:H through mixed-phase Si:H to nc-Si:H; the film prepared with R=50 (right) nucleates immediately from the substrate as nc-Si:H. (*R* is the ratio of the H_2 and the SiH_4, see Table 1.).

The polycrystalline CdS and CdTe thin films were magnetron sputtered onto ~ 10 x 15 cm^2 Mo-covered soda lime glass (SLG/Mo/CdTe/CdS) [43]

The thin films were measured during deposition in-situ and in real-time using a rotating-compensator multichannel spectroscopic ellipsometer (J.A. Woollam Co., M-2000DI) at one point close to the center of the 15 x 15 cm^2 (Si:H films) or the 10 x 15 cm^2 (CdTe/CdS films) samples. The single-spot measurements of a series of ellipsometric spectra obtained versus time during deposition permit the development of an appropriate multilayer optical model, which provides starting parameters in least-squares regression for the analysis of the mapping data acquired by our prototype spectroscopic ellipsometer for imaging/mapping purposes. To check our mapping expanded beam SE results, we performed mapping SE measurements and evaluations (using the same optical models and wavelength regions) by an AccuMap device (by J.A. Woollam Co) ex-situ.

RESULTS AND DISCUSSION

The dual-spectral prototype were designed to enable in situ imaging/mapping within one of the chambers of a cluster tool at the Center for Photovoltaics Innovation and Commercialization (PVIC); University of Toledo (Ohio), see Fig. 2.

Calibration and validating measurements

Calibration and validating measurements were performed on nominally 20, 40, 60 and 80 nm thermal oxide covered 6-inch Si-wafers. The results were compared with AccuMap results, see Figure 7.

Demonstration measurements

Silicon layers

Poly-Si layer (poly-Si 46) on SiO_2 on 6-inch Si-wafer (prepared by LPCVD) were measured by AccuMap and expanded beam device line-by-line (1 X-point = 1 cm) and during continuous moving (1 X-point ~ 1.5 cm). The calculated thickness-maps are shown in Fig. 8 and a very good agreement can be established.

Demonstration mapping measurements have been performed ex situ on mixed-phase (a-Si:H + nc-Si:H) silicon films having the structure: nc-Si/(nc-Si+a-Si)/a-Si/Cr/glass. Imaging/mapping for initial demonstration purposes, however, was performed on a single phase a-Si:H/Cr/glass sample (see Fig. 9) and compared with independent mapping measurements made by a commercially-available instrument (AccuMap) that is capable of point-by-point mapping measurements on larger size samples. With intentionally extreme settings of the deposition parameters, a purely amorphous layer with high spatial non-uniformity was prepared in order to demonstrate the utility of our method. A relatively simple optical model was used to analyze the mapping measurement: opaque Cr as a substrate, and a-Si:H with a Tauc-Lorentz oscillator dispersion model. The parameters of the Tauc-Lorentz oscillator were taken from the real time SE measurement.

We performed the second evaluation of the mapping measurement using the R=20 sample of Table 1 (see Fig. 10) and applying a 3-layer optical model consisting of the following stack: nc-Si:H/(a-Si:H+nc-Si:H)/a-Si:H/Cr, which was developed from single-spot, real-time spectroscopic ellipsometry (SE) analysis [44]. In addition to the appropriate model, this real time SE measurement also provided good starting parameters in least-squares regression for the analysis of the mapping data using the model. We also compared our mapping results with the results (using the same optical model) of independently performed ex-situ measurements with the AccuMap (see Fig. 10). We must note that this latter instrument obtains ellipsometric spectra at mm-size spots on a square grid, whereas the expanded-beam instrument obtains spectra for ~ 5 x 5 mm_2 areas. So, we cannot ensure that the individual ellipsometers are collecting spectra from precisely the same areas with the same resolution.

The agreement in Fig. 10 is very good, considering the complexity of the model, consisting of three individual Si:H layers. The circular areas of reduced thickness on the maps arise from the use of a top cathode plate with two holes that permit passage of the beam for real time SE. When larger area devices are made, these specialized electrodes are replaced with standard ones.

SLG/Mo/CdTe/CdS

The magnetron sputtered polycrystalline CdS and CdTe thin films were modelled by dielectric functions taken from real time SE measurement and the model contained surface roughness and interface layers, too. We show only the thickness of the CdTe layer and the "Total thickness" (all layers in the models, including the surface roughness and interface layers) in Fig. 11. Unfortunately, we had a problem with the sample holder (because of the continuous changing of the rigid sample holders and the cassette roll-to-roll model machine) so we could measure only the central part of the sample by the imaging instrument.

One remark: if the lateral change (inhomogeneity) is well over 1 nm/mm then the expanded beam ellipsometer does not measure the same thing as single spot ellipsometers! In the case of 80 nm thick SiO_2 film the inhomogeneity is: 6 nm/6 cm = 0.1 nm/mm, so the inhomogeneity within the expanded beam SE's elementary area is 0.5 nm. In the case of the polysilicon sample the inhomogeneity is 50 nm/6 cm =0.8 nm/mm, so the inhomogeneity within the expanded beam SE's elementary area is 4 nm. In the case of the CdTe/CdS sample the inhomogeneity is 300 nm/4 cm =7.5 nm/mm, so the inhomogeneity within the expanded beam SE's elementary area is 40 nm! However, the difference between the mapping results is below 1 % in all cases.

In-line roll-to-roll (RtR) measurement

We measured a ZnO layer (deposited by magnetron sputtering onto an Ag-covered plastic foil in a cassette roll-to-roll model machine) in-line by the expanded beam device, see Fig. 12. We used a simple Cauchy-dispersion for the ZnO layer because of the limited wavelength region, see the selected spectra (measured and fitted) in Fig. 12. Note the larger MSE values at the edges of the sample!

In another experiment, we measured first a ZnO only (on Ag layer/plastic foil) RtR sample and moved the cassette roll-to-roll model machine into the a-Si deposition chamber. After the a-Si deposition the cassette roll-to-roll model machine was moved back to the measuring chamber (without breaking the vacuum) and measured again by the expanded beam mapping SE, see Fig. 13. Mapping SE was performed from the leading end of the roll, counter-clockwise (CCW) first and clockwise (CW) after the a-Si deposition. We have got the same map for the ZnO layer and we can see the same greater MSE values at the "wrinkled" line of the foil! This "wrinkle" cause a similar effect as the edges of the foil, possibly making the angles of incidence locally different from the calibrated ones. This effect shows that our expanded beam mapping SE is a robust device which is relatively insensitive for the small distortions.

Present status and near future plans

The dual-spectral prototype (enhanced with a rotating compensator option) is working as an in situ imaging/mapping device (currently a single 40 point line image can be collected in 10 sec over a 15 cm width of PV material) within one of the chambers of a cluster tool at the Center for Photovoltaics Innovation and Commercialization (PVIC) University of Toledo (Ohio)

Currently, a single-spectrum (350-1000 nm, with a rotating compensator) instrument for 30-cm sample-size is completed at MFA (Budapest, Hungary) and it is under calibration. (See Fig. 14) Our group is involved in a domestic project (supported by the Hungarian Government) in consortium with a Hungarian company (Tenzi Ltd.). Our goal is to develop prototypes of expanded beam ellipsometers for applications in solar cell industry, and in the next 2 years (2013-2014) we plan to fabricate prototypes for 60-cm (end of 2013) and 90-cm sample-size (2014). These instruments will measure the single-spectrum (350-1000 nm) within 5 sec.

CONCLUSIONS

Thin film PV is more cost effective than bulk PV technology, but higher efficiency needs lateral homogeneity! Commercial instruments using 1D detector arrays for spectroscopic ellipsometry must translate either the sample or the ellipsometer in two dimensions in order to map large area samples. A 15 x 15 cm2 sample requires > 200 measurements and at least 15 min of measurement time to achieve cm scale spatial resolution. By using a 2D detector array and imaging along one dimension in parallel, the sample need only be translated in one dimension in order to map large area samples. As a result, our expanded-beam system (that provides a line image of spectroscopic (350-1000 nm) ellipsometry) data can measure with similar spatial resolution in < 2 min. (Currently a single 40 point line image can be collected in 10 s over a 15 cm width of PV material.) Incorporating the results of real time SE measurements, which provide good starting parameters in least-squares regression for the analysis of the imaging/mapping data, expanded-beam ellipsometry can be an effective in-line monitor of uniformity in PV production lines using roll-to-roll or rigid plate substrates. The goal of near future (2 years) efforts is to increase the speed by 10x and scale up the width by 4x. Then 1800 points could be mapped in a 1 min traverse of a (60*120 cm) PV panel.

ACKNOWLEDGMENTS

This work was supported by the National Development Agency KMR_12_1_2012_0225 project, ENIAC “E450EDL” and grant TAMOP-4.2.2/B-10/1-2010-0025

References

[1] H. Fujiwara, *Spectroscopic Ellipsometry: Principles and Applications*, Wiley (2007)

[2] H. G. Tompkins, E. A. Irene (eds.), *Handbook of Ellipsometry*, William Andrew Publishing (2005)

[3] M. Losurdo, K. Hingerl (eds.), *Ellipsometry at the Nanoscale*, Springer (2013)

[4] T. Lohner, N. Q. Khánh, Z. Zolnai; Spectroellipsometric characterization of ion implanted semiconductors and porous silicon; Acta Phys. Slovaca 48 (1998) 441-450.

[5] M. Serényi, T. Lohner, P. Petrik, C. Frigeri, Comparative analysis of amorphous silicon and silicon nitride multilayer by spectroscopic ellipsometry and transmission electron microscopy, Thin Solid Films 515 (2007) 3559-3562.

[6] M. Serenyi, T. Lohner, P. Petrik, Z. Zolnai, Z.E. Horvath, N.Q. Khanh, Characterization of sputtered and annealed niobium oxide films using spectroscopic ellipsometry, Rutherford backscattering spectrometry and X-ray diffraction, Thin Soild Films 516 (2008) 8096-8100.

[7] P. Petrik, Ellipsometric models for vertically inhomogeneous composite structures, Phys. Status Solidi A 205 (2008) 732-738

[8] T. Lohner, A. Szekeres, T. Nikolova, E. Vlaikova, P. Petrik, G. Huhn, K. Havancsak, I. Lisovskyy, S. Zlobin, I. Z. Indutnyy, P. E. Shepeleliavyi, Optical models for ellipsometric characterization of high temperature annealed nanostructured SiO2 films, J. Optoelectorn. Adv. Mater. 11 (2009) 1288-1291.

[9] A. Szekeres, T. Lohner, P. Petrik, G. Huhn, K. Havancsak, I. Lisovskyy, S. Zlobin, I. Z. Indutnyy, P. E. Shepeliavyi, Ellipsometric characterization of SiOx films with embedded Si nanoparticles, Vacuum 84 (2009) 115-118

[10] T. Lohner, A. Pongracz, N.Q. Khanh, O.H. Krafcsik, K.V. Josepovits, P. Deak P, Comparative investigation of the Si/SiO_2 interface layer containing SiC crystallites using spectroscopic ellipsometry, ion beam analysis and XPS, Phys. Status Solidi C 5 (2008) 1337-1340.

[11] P. Kozma, B. Fodor, A. Deak, P. Petrik, Optical Models for the Characterization of Silica Nanosphere Monolayers Prepared by the Langmuir-Blodgett Method Using Ellipsometry in the Quasistatic Regime, Langmuir 26 (2010) 16122.

[12] P. Petrik, "*Characterization of Nanocrystals Using Spectroscopic Ellipsometry*", In: Sudheer Neralla (ed.), "Nanocrystals - Synthesis, Characterization and Applications", InTech, 2012, 29-40

[13] L.R. Dahal, Z.Huang, D. Attygalle, C. Salupo, S. Marsillac, N.J. Podraza, R.W. Collins. Correlations between Mapping Spectroscopic Ellipsometry Results and Solar Cell Performance for Evaluations of Non-Uniformity in Thin Film Silicon Photovoltaics, IEEE J. Photovolt. 3 (2013) 387-393

[14] Aryal, P., Attygalle, D., Pradhan, P., Podraza, N.J., Marsillac, S., Collins, R.W.; Large-Area Compositional Mapping of Cu(In{1-x}Ga{x})Se{2} Materials and Devices with Spectroscopic Ellipsometry, IEEE J. Photovolt. 3 (2013) 359-363

[15] A.M. Hermann, C. Gonzalez, P.A. Ramakrishnan, D. Balzar, C.H. Marshall, J.N. Hilfiker, T. Tiwald, Growth and characterization of large area Cu(*In*,Ga)Se2 films, Thin Solid Films 387 (2001) 54-56

[16] M.I. Alonso, M. Garriga, C.A. Durante Rincon, E.Hernandez, M. Leon, Optical functions of chalcopyrite Cu $Ga_xIn_{1-x}Se_2$ alloys, Appl. Phys. A 74 (2002) 659–664

[17] S. Minoura, K. Kodera, T. Maekawa, K. Miyazaki, S. Niki, H. Fujiwara, Dielectric function of Cu(In, Ga)Se_2-based polycrystalline materials, J. Appl. Phys. 113 (2013) 063505

[18] J. Li, D. Levi, M. Contreras, J. Scharf, Optiocal control of multi-stage thin film solar cell production, United States Patent Application US/SN 61/778,079, Filed March 12, 2013:

[19] J. Li, J. Chen, R. W. Collins, Broadening of optical transitions in polycrystalline CdS and CdTe thin films, Appl. Phys. Lett. 97 (2010) 181909

[20] J. Li, J. Chen, R.W. Collins, Optical transition energies as a probe of stress in polycrystalline CdTe thin films, Appl. Phys. Lett. 99 (2011) 061905

[21] P. I. Rovira, R. W. Collins, Analysis of specular and textured SnO2:F films by high speed four-parameter Stokes vector spectroscopy, J. Appl. Phys. 85 (1999) 2015

[22] H. Fujiwara, M. Kondo, Effects of carrier concentration on the dielectric function of ZnO:Ga and In2O3:Sn studied by spectroscopic ellipsometry: Analysis of free-carrier and band-edge absorption, Phys. Rev. B 71 (2005) 075109

[23] M. Akagawa, H. Fujiwara, High-precision characterization of textured a-Si:H/SnO2:F structures by spectroscopic ellipsometry, J. Appl. Phys. 110 (2011) 073518

[24] H. Yoshikawa, S. Adachi, Optical Constants of ZnO, Japanese J. Appl. Phys. 36 (1997) 6237

[25] C. Major, A. Nemeth, G. Radnoczi, Zs. Czigany, M. Fried, Z. Labadi, I. Barsony, Optical and electrical characterization of aluminium doped ZnO layers, Appl. Surf. Sci. 255 (2009) 8907-8912

[26] S. Kageyama, M. Akagawa, H. Fujiwara; Dielectric function of a-Si:H based on local network structures, Phys. Rev. B 83 (2011) 195205

[27] W. Guter, J. Schöne, S. P. Philipps, M. Steiner, G. Siefer, A. Wekkeli, E. Welser, E. Oliva, A. W. Bett, F. Dimroth, Current-matched triple-junction solar cell reaching 41.1% conversion efficiency under concentrated sunlight, Appl. Phys. Lett. 94 (2009) 223504

[28] A. Luque, Will we exceed 50% efficiency in photovoltaics? J. Appl. Phys. 110 (2011) 031301

[29] S. Wojtczuk, P. Chiu, X. Zhang, D. Derkacs, C. Harris, D. Pulver, and M. Timmons, InGaP/GaAs/InGaAs 41% concentrator cells using bi-facial epigrowth, in: Proceedings of the 35th IEEE Photovoltaic Specialists Conf. (2010) pp.1259–1264

[30] M P Suryawanshi, G L Agawane, S M Bhosale, S W Shin, P S Patil, J H Kim, A V Moholkar, CZTS based thin film solar cells: a status review, Materials Technology, 28 (2013) 98–109

[31] T.K. Todorov, J. Tang, S. Bag, O. Gunawan, T. Gokmen, Y. Zhu, D. B. Mitzi, *Beyond 11% Efficiency: Characteristics of State-of-the-Art Cu2ZnSn(S,Se)4 Solar Cells,* Adv. Energy Mater. 3 (2013) 34–38

[32] H. X. Wang, Progress in Thin Film Solar Cells Based on Cu2ZnSnS4, Int. J. Photoenergy, 2011 (2011) 801292

[33] T. Omata, K. Nose, S. Otsuka-Yao-Matsuo, Size dependent optical band gap of ternary I-III-VI2 semiconductor nanocrystals, J. Appl. Phys. 105 (2009) 073106

[34] S. L. Castro, S. G. Bailey, R. P. Raffaelle, K. K. Banger, A. F. Hepp, Synthesis and Characterization of Colloidal $CuInS_2$ Nanoparticles from a Molecular Single-Source Precursor, J. Phys. Chem. B 108 (2004) 12429

[35] K. Nose , Y. Soma , T. Omata, S. Otsuka-Yao-Matsuo, Synthesis of Ternary $CuInS_2$ Nanocrystals; Phase Determination by Complex Ligand Species, Chem. Mater. 21 (2009) 2607

[36] S. Wippermann, M. Vörös, D. Rocca, A. Gali, G. Zimanyi, and G. Galli, High-Pressure Core Structures of Si Nanoparticles for Solar Energy Conversion, Phys. Rev. Lett. 110 (2013) 046804

[37] M. Vörös, D. Rocca, G. Galli, G. T. Zimanyi, A. Gali; Increasing impact ionization rates in Si nanoparticles through surface engineering: A density functional study, Phys. Rev. B 87 (2013) 155402

[38] Z. G. Horváth, G. Juhász, M. Fried, C. Major, P. Petrik, Imaging Optical Inspection Devide with a Pinhole Camera, U.S. Patent No. 8437002 B2, 25 Nov. 2010.

[39] G. Juhasz, Z. Horvath, C. Major, P. Petrik, O. Polgar, M. Fried, Non-collimated beam ellipsometry, Phys. Stat. Sol. (c) 5 (2008) 1081-1084

[40] C. Major, G. Juhasz, Z. Horvath, O. Polgar, M. Fried, Wide angle beam ellipsometry for extremely large samples, Phys. Stat. Sol. (c) 5 (2008) 1077-1080

[41] C. Major, G. Juhasz, P. Petrik, Z. Horvath, O. Polgar, M. Fried, Application of wide angle beam spectroscopic ellipsometry for quality control in solar cell production, Vacuum 84 (2009) 119-122

[42] M. Fried, G. Juhasz, C. Major, P. Petrik, O. Polgar, Z. Horvath, A. Nutsch, Expanded beam (macro-imaging) ellipsometry, Thin Solid Films 519 (2011) 2730-2736

[43] J. Li, J. Chen, M. N. Sestak, C. Thornberry, R. W. Collins, Spectroscopic ellipsometry studies of thin film CdTe and CdS: from dielectric functions to solar cell structures, 34th IEEE Photovolt. Specialists Conf. 1-3 (2009) pp. 1783-1788

[44] R. W. Collins, A. S. Ferlauto, G. M. Ferreira, C. Chen, J. Koh, R. J. Koval, Y. Lee, J. M. Pearce, C. R. Wronski, Evolution of microstructure and phase in amorphous, protocrystalline, and microcrystalline silicon studied by real time spectroscopic ellipsometry, Sol. Energy Mater. Sol. Cells 78 (2003) 143-180

List of figure captions:

Figure 1: (1) “white” light source, (2) narrow, rectangular aperture, (3) film-polarizer, (4) compensator, (5) spherical mirror (6) sample, (7) cylindrical mirror, corrected beam, (8) analyzer, (9) pinhole, (10) correction-dispersion optics, (11) CCD detector array.

Figure 2: The prototype CAD-drawing (upper), located within the Center for Photovoltaics Innovation and Commercialization at the University of Toledo (Ohio), earlier operating in an ex situ mode (middle), presently integrated into a multichamber cluster tool for in situ analysis (bottom).

Figure 3 100 nm oxide: Δ is near 180 deg. Comparison of rotating Polarizer (left) and rotating Compensator (right) measurements

Figure 4: Comparison of rotating Polarizer and rotating Compensator measurement (nominally 1450 nm thick oxide layer)

Figure 5: Fit of rotating Compensator measurement (nominally 1350 nm thick oxide layer)

Figure 6: XTEM images for a sample prepared at R=20 (left; MCS 25) and one prepared at R=50 (right; MCS 26). The substrate is seen in the upper-left corner. The a-Si:H, mixed-phase (a-Si:H + nc-Si:H), and nc-Si:H sub-layers can be seen in the R=20 sample from the upper to lower part of the image.

Figure 7: Calibrating and validating measurements on thermal oxides (nominal thickness: 20, 40, 60 and 80 nm) (differences between expanded beam (left) and AccuMap (right) ≤ 1 nm) Only the center line is used for calibration, the other points considered as checking. Points at the corners are from spectra measured on partly the sample and mainly on the holder.

Figure 8: Thickness-map of poly-Si layer on SiO2 on 6-inch Si-wafer by AccuMap (top left), desk-top expanded beam device line-by-line (stop during measurement, top middle) and expanded beam device line-by-line during continuous moving, respectively (top-right). The used optical model (effective medium approximation with c-Si/a-Si mixture) and a sample spectrum-pair (with model fit) from a central sample-position is shown in the bottom row. Measured ellipsometric spectra shown in the bottom row are from the continuously moving/mapping.

Figure 9: Mapping with a commercial instrument (left) and imaging/mapping with an expanded beam instrument (right) showing reasonable agreement; thickness maps in nm were obtained for a 15 x 15 cm2 size sample of single-phase hydrogenated amorphous silicon (a-Si:H) layer on Cr. The map generated by the commercial instrument denotes points on a square grid at the sample surface; the map generated by the expanded-beam ellipsometer is described in terms of pixelgroup coordinates.

Figure 10: Mapping with a commercial instrument and imaging/mapping with the expanded-beam instrument for an thin Si:H film with R=20 using the 3-layer optical model given by nc-Si:H/(a-Si:H+nc-Si:H)/a-Si:H /Cr. The total thickness is the sum of the thicknesses of the three sub-layers for each spatial point.

Figure 11: Mapping with the AccuMap (left) and imaging/mapping with the expanded-beam instrument (right) for a SLG/Mo/CdTe/CdS sample. The total thickness is the sum of the thicknesses including the surface roughness and interface layers for each spatial point.

Figure 12: ZnO layer (deposited by magnetron sputtering onto Ag-covered plastic foil in a cassette roll-to-roll model machine) measured in-line by the expanded beam device. (Upper part) The horizontal axis is the direction of web advance. Mapping SE was performed from the leading end of the roll. The vertical axis is the width of the web, from which the edge-to-edge uniformity of the film deposition is evaluated. The gradient at the starting and ending parts is due to the sinΘ/r2 dependence of the flux. Thickness-map (middle, left), An-map (middle, right), MSE-map (bottom, right) Result of the selected (1 elementary point) expanded beam

mapping SE measurement: MSE=0.059, Thickness=326.6 ± 8 nm, An=1.80 ± 0.03, Bn=- 0.003 ± 0.0047, Cn=0.007 ± 0.0007, Ak=0.017 ± 0.007, Bk=1.44 ± 0.6 (bottom, left)

Figure 13 Thickness-map (upper-left) and MSE-map (upper-center) of the ZnO layer (deposited by magnetron sputtering onto Ag-covered plastic foil in a cassette roll-to-roll model machine, upper-right) and Thickness-map (bottom-left) of a-Si layer and Thickness-map (bottom-left) of ZnO layer and MSE-map (bottom-right). The a-Si layer was deposited after the first measurement. Measurements were performed in-line by the expanded beam device. The horizontal axis is the direction of web advance (in cm steps). Mapping SE was performed from the leading end of the roll, counter-clockwise (CCW) first and clockwise (CW) after the a-Si deposition. Note, the greater MSE values at the "wrinkled" line of the foil!

Figure 14 Single-spectrum (350-1000 nm), rotating compensator expanded beam SE mapping device for 30-cm sample-size is completed at MFA (Budapest, Hungary); CAD-drawing with the beam-path (left) and photograph (right)

Table 1 Deposition parameters of the Si:H samples prepared onto Si wafer and Cr-coated SLG substrates.

Sample no.	Time [min]	Pressure [Pa]	RF power [W]	SiH_4 [sccm]	H_2 [sccm]	R (H_2/SiH_4)
MCS 23	10	40	4	10	5	0.5
MCS 25	20	200	40	5	100	20
MCS 26	20	200	40	5	250	50

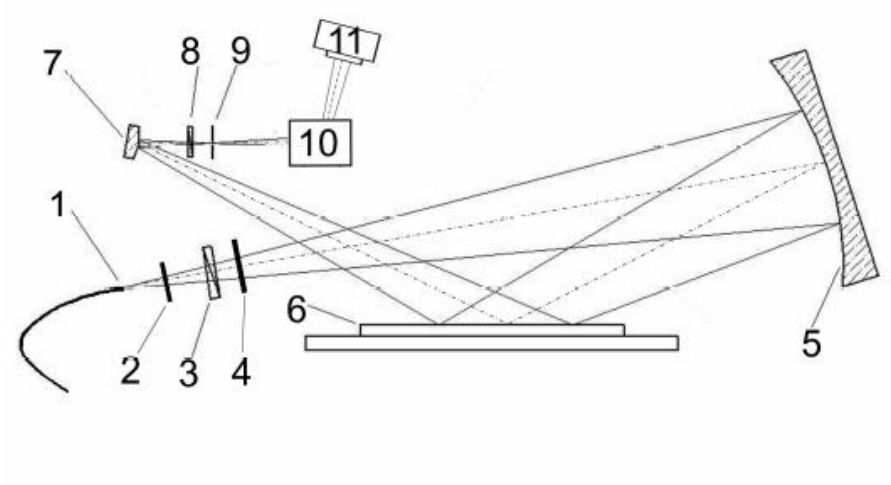

***Figure 1**: (1) "white" light source, (2) narrow, rectangular aperture, (3) film-polarizer, (4) compensator, (5) spherical mirror (6) sample, (7) cylindrical mirror, corrected beam, (8) analyzer, (9) pinhole, (10) correction-dispersion optics, (11) CCD detector array.*

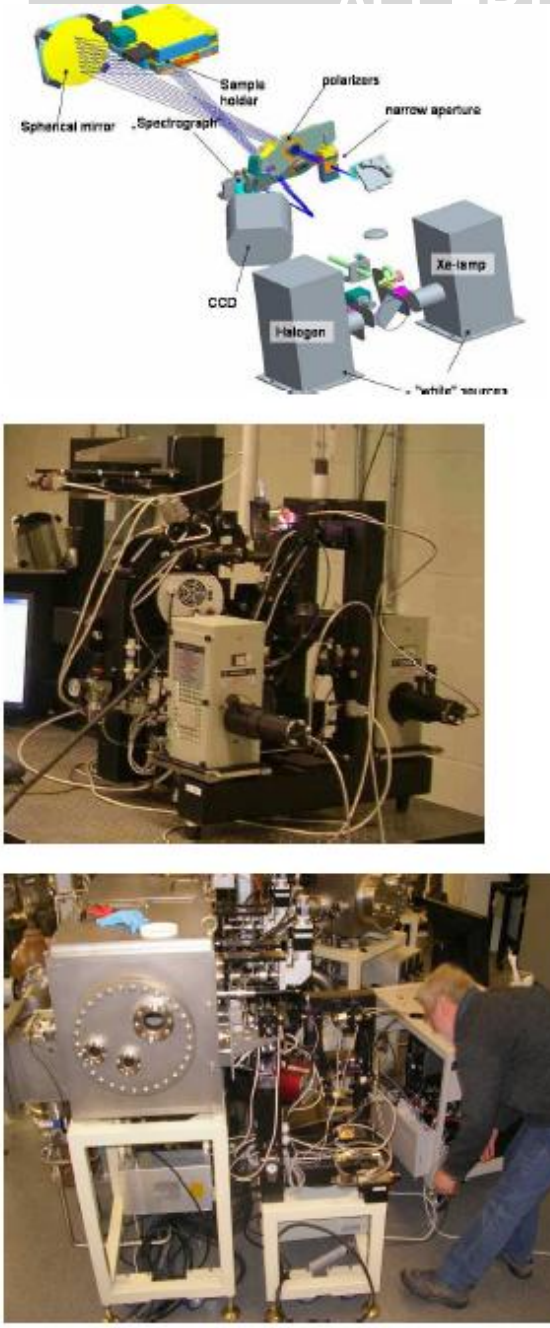

Figure 2 *The prototype CAD-drawing (upper), located within the Center for Photovoltaics Innovation and Commercialization at the University of Toledo (Ohio), earlier operating in an ex situ mode (middle), presently integrated into a multichamber cluster tool for in situ analysis (bottom).*

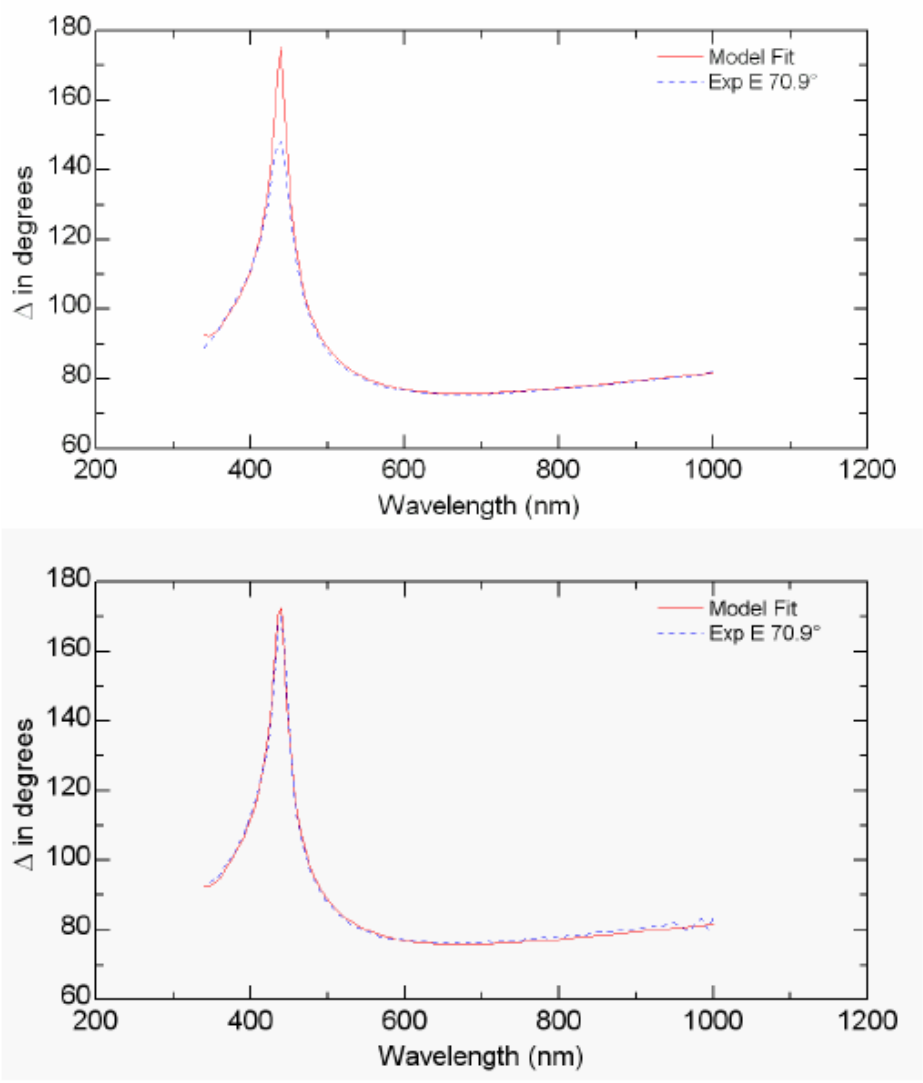

Figure 3 *100 nm oxide: Δ is near 180 deg. Comparison of rotating Polarizer (left) and rotating Compensator (right) measurements*

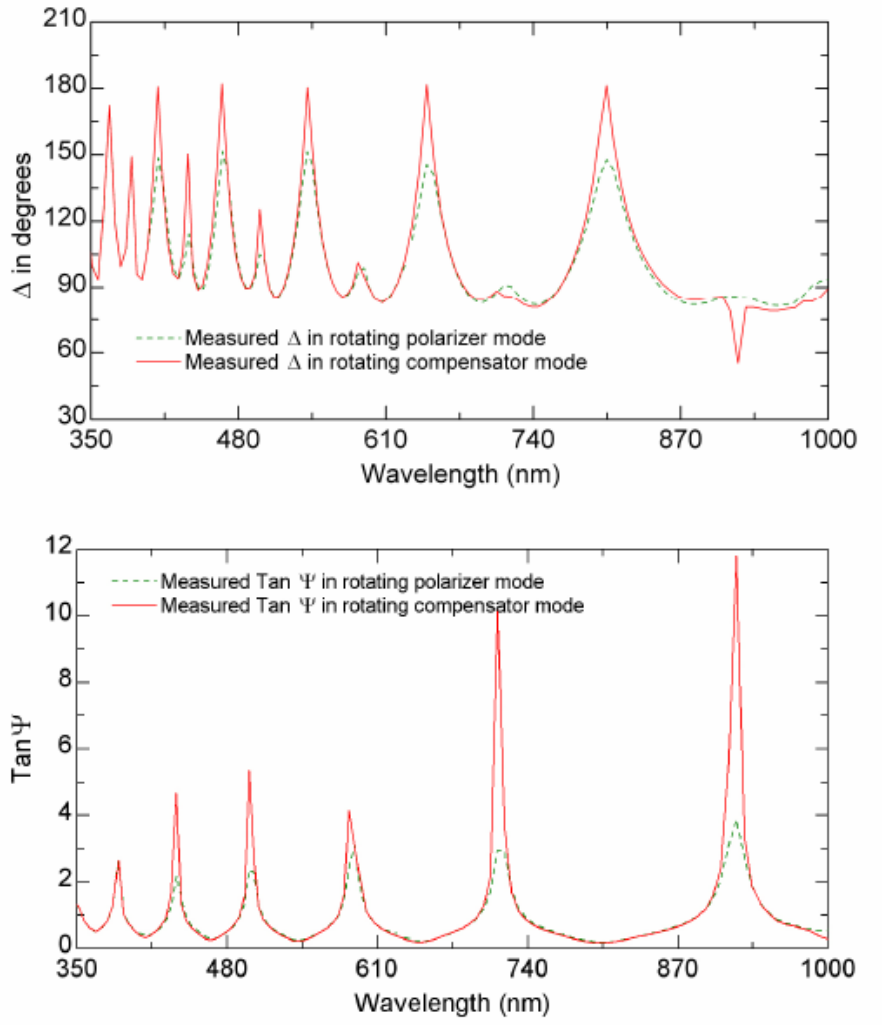

Figure 4 *Comparison of rotating Polarizer and rotating Compensator measurement (nominally 1450 nm thick oxide layer)*

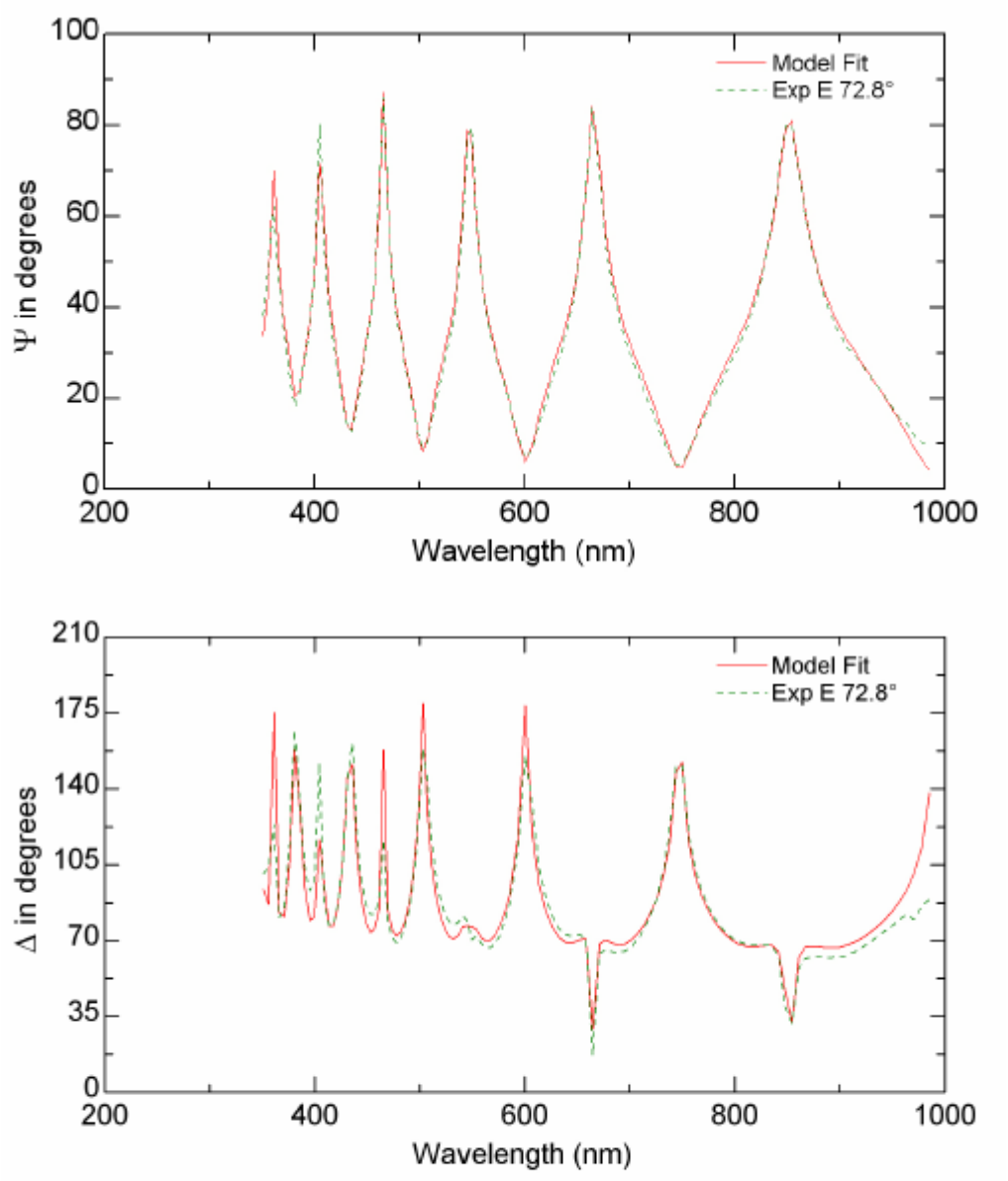

Figure 5 *Fit of rotating Compensator measurement (nominally 1350 nm thick oxide layer)*

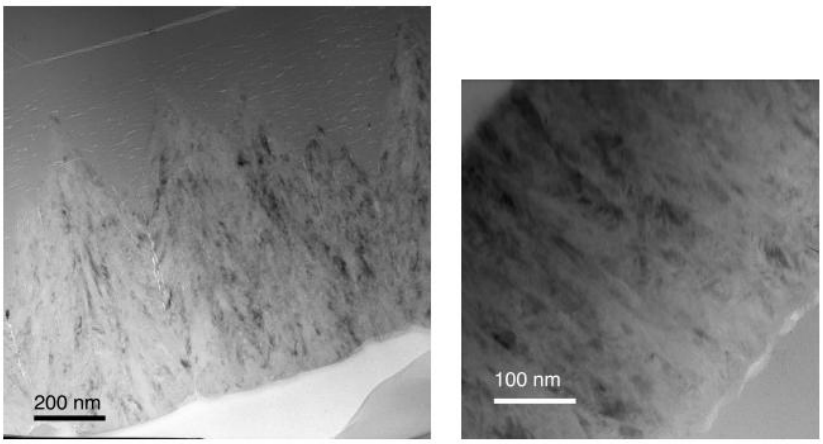

Figure 6: *XTEM images for a sample prepared at R=20 (left; MCS 25) and one prepared at R=50 (right; MCS 26). The substrate is seen in the upper-left corner. The a-Si:H, mixed-phase (a-Si:H + nc-Si:H), and nc-Si:H sub-layers can be seen in the R=20 sample from the upper to lower part of the image.*

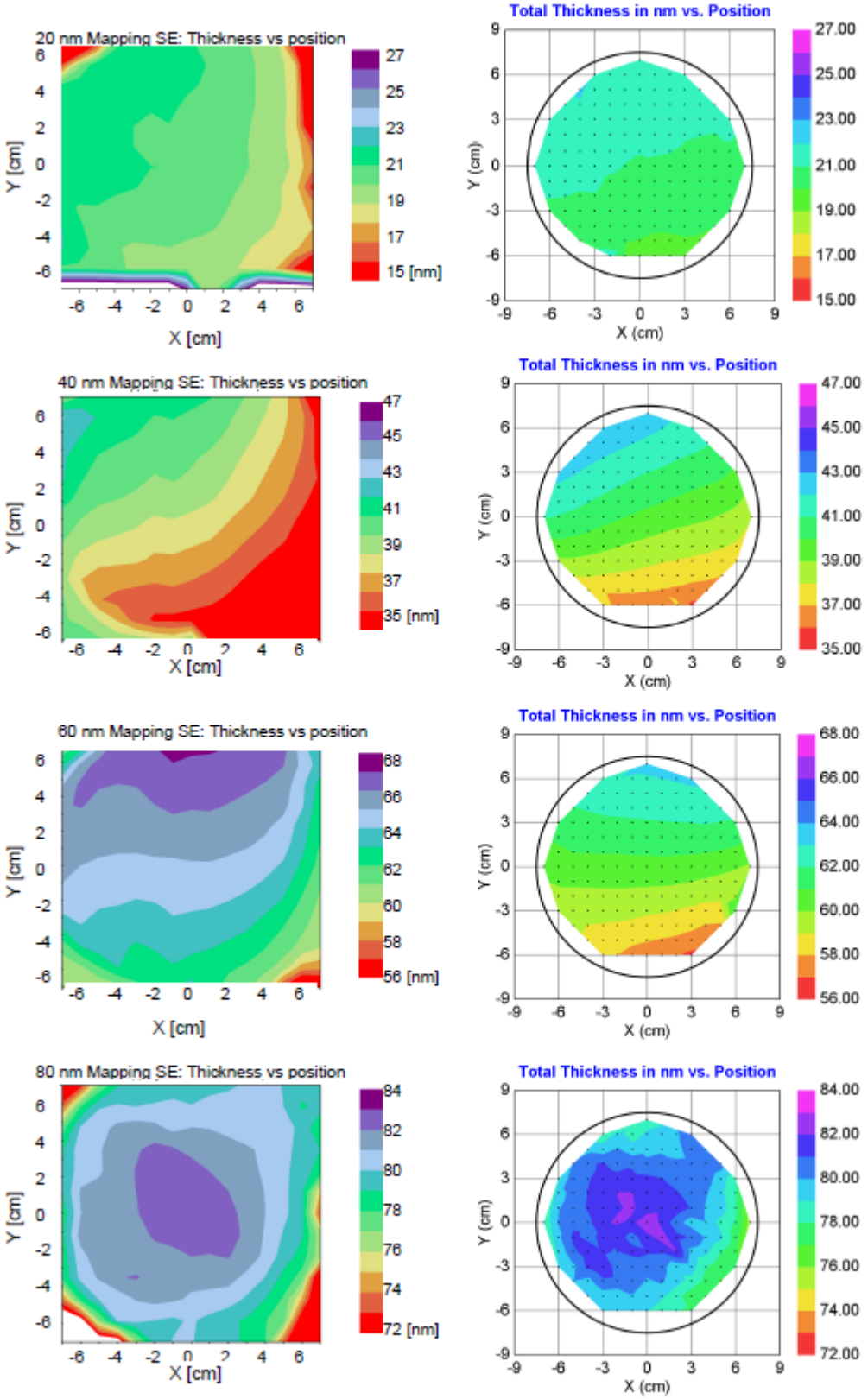

Figure 7 *Calibrating and validating measurements on thermal oxides (nominal thickness: 20, 40, 60 and 80 nm) (differences between expanded beam (left) and AccuMap (right) ≤ 1 nm) Only the center line is used for calibration, the other points considered as checking. Points at the corners are from spectra measured on partly the sample and mainly on the holder.*

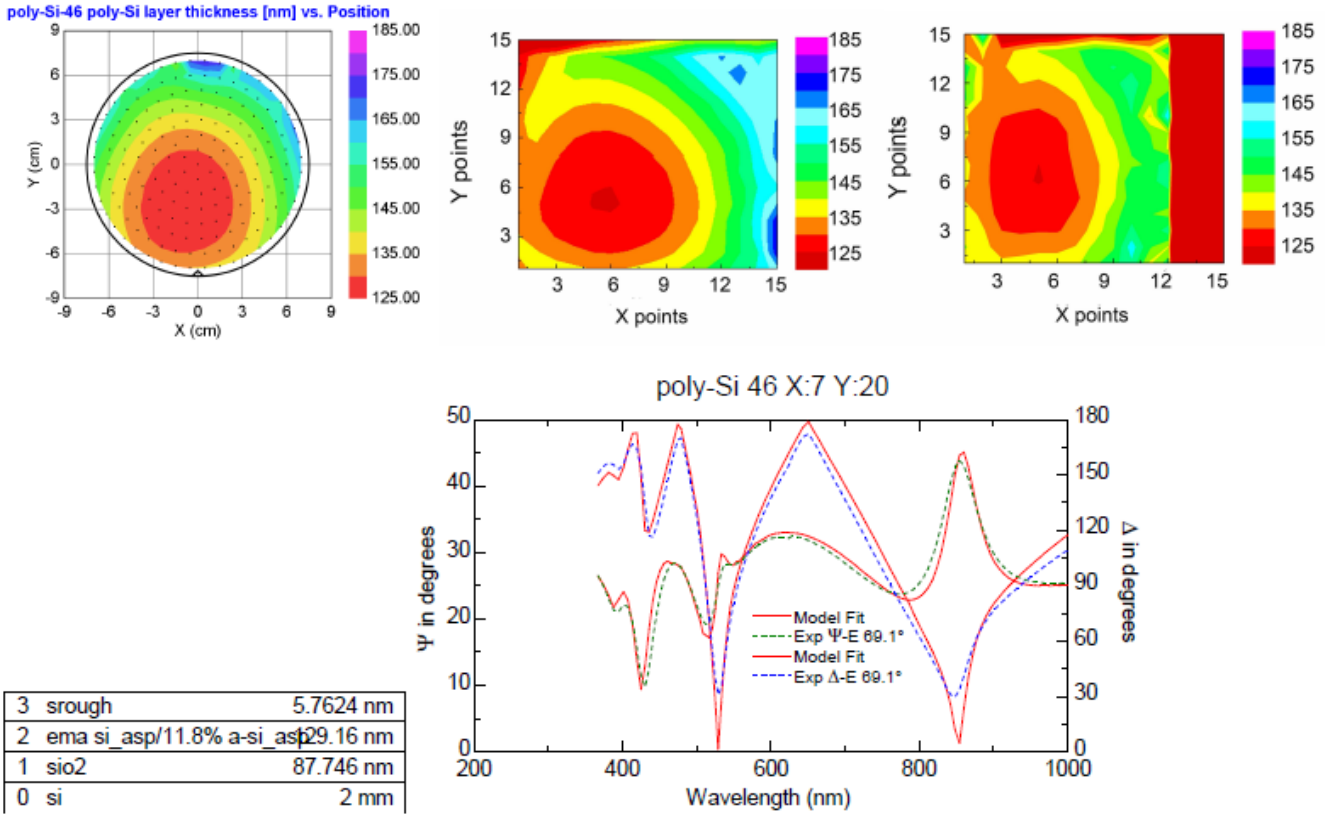

3	srough	5.7624 nm
2	ema si_asp/11.8% a-si_asp	29.16 nm
1	sio2	87.746 nm
0	si	2 mm

Figure 8 *Thickness-map of poly-Si layer on SiO_2 on 6-inch Si-wafer by AccuMap (top left), desk-top expanded beam device line-by-line (stop during measurement, top middle) and expanded beam device line-by-line during continuous moving, respectively (top-right). The used optical model (effective medium approximation with c-Si/a-Si mixture) and a sample spectrum-pair (with model fit) from a central sample-position is shown in the bottom row. Measured ellipsometric spectra shown in the bottom row are from the continuously moving/mapping.*

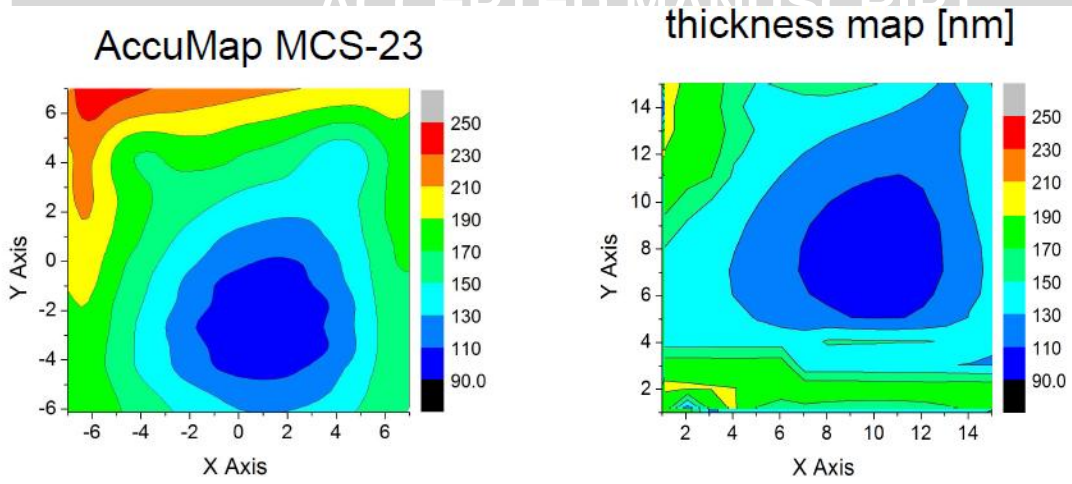

Figure 9 *Mapping with a commercial instrument (left) and imaging/mapping with an expanded beam instrument (right) showing reasonable agreement; thickness maps in nm were obtained for a 15 x 15 cm^2 size sample of single-phase hydrogenated amorphous silicon (a-Si:H) layer on Cr. The map generated by the commercial instrument denotes points on a square grid at the sample surface; the map generated by the expanded-beam ellipsometer is described in terms of pixel-group coordinates.*

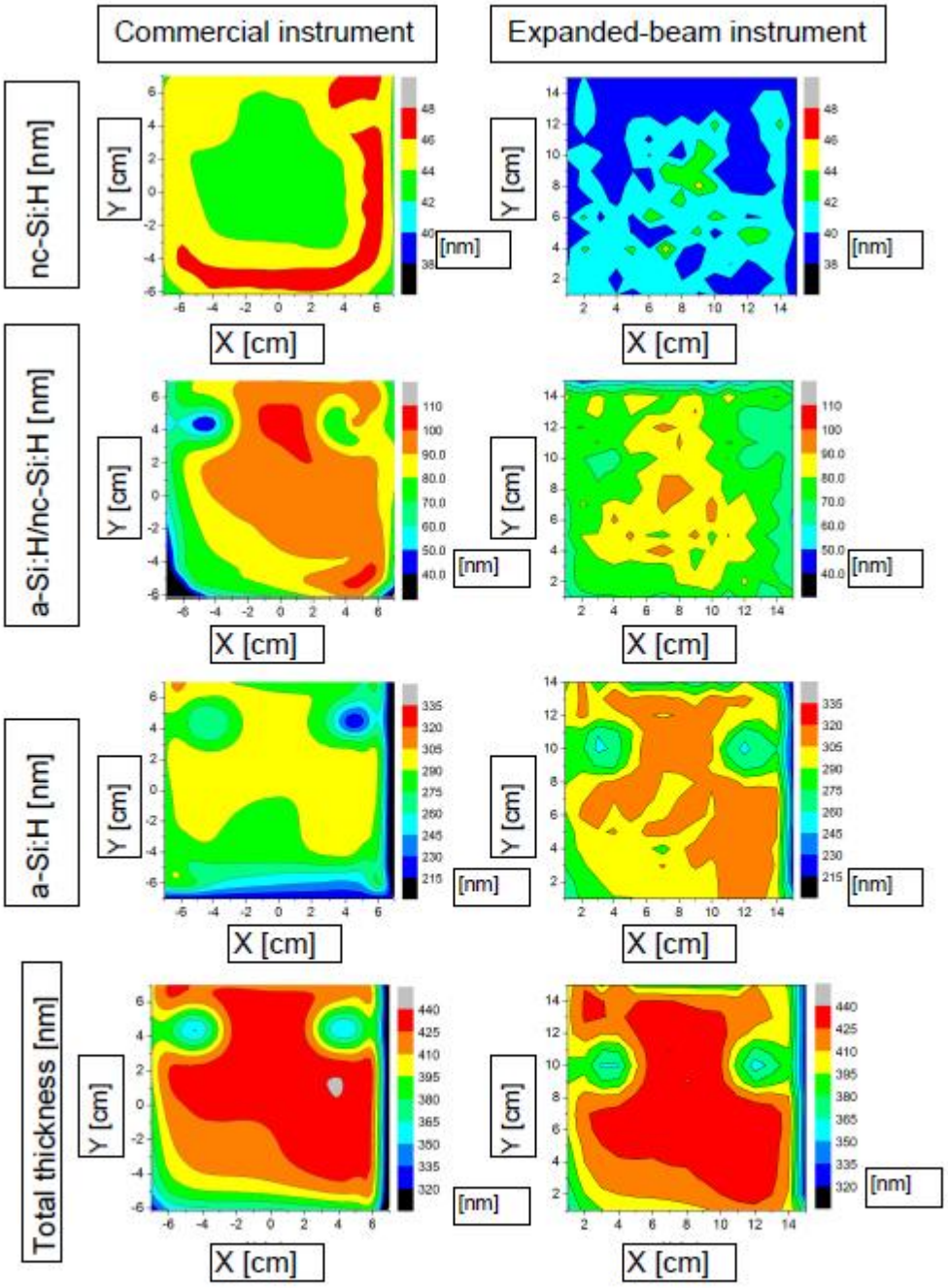

Figure 10 *Mapping with a commercial instrument and imaging/mapping with the expanded-beam instrument for an thin Si:H film with R=20 using the 3-layer optical model given by nc-Si:H/(a-Si:H+nc-Si:H)/a-Si:H /Cr. The total thickness is the sum of the thicknesses of the three sub-layers for each spatial point.*

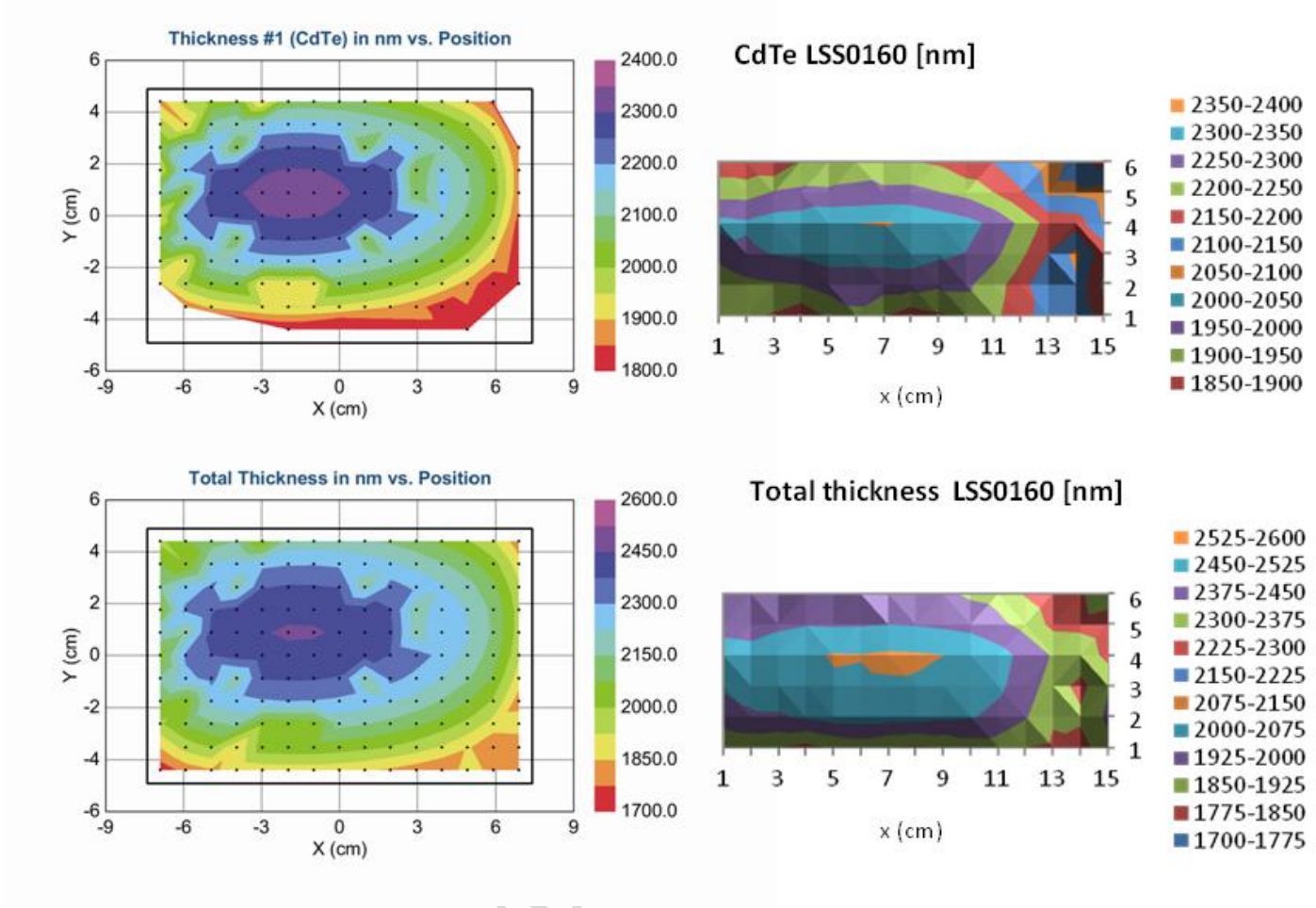

Figure 11

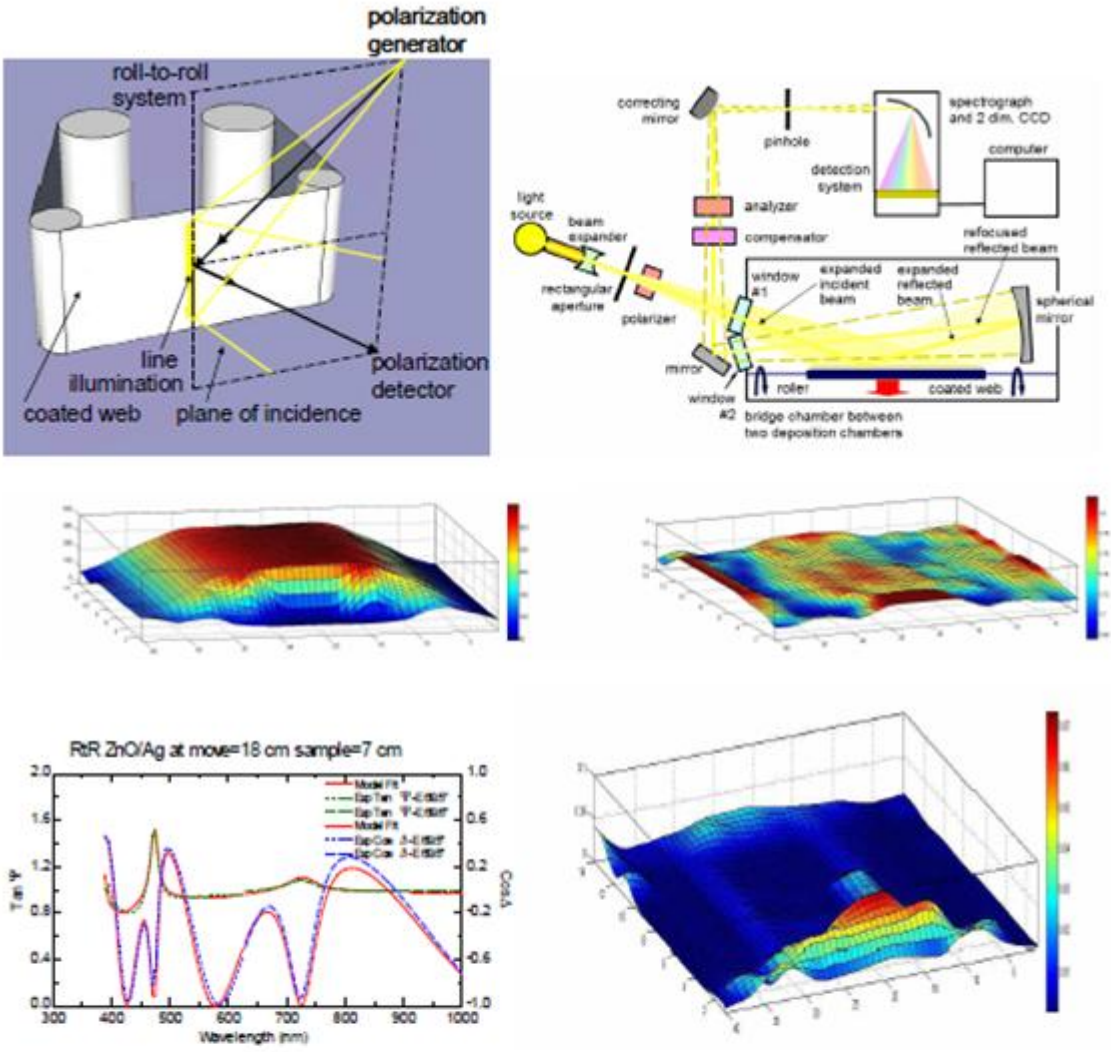

Figure 12 *ZnO layer (deposited by magnetron sputtering onto Ag-covered plastic foil in a cassette roll-to-roll model machine) measured in-line by the expanded beam device. (Upper part) The horizontal axis is the direction of web advance. Mapping SE was performed from the leading end of the roll. The vertical axis is the width of the web, from which the edge-to-edge uniformity of the film deposition is evaluated. The gradient at the starting and ending parts is due to the* $\sin\Theta/r^2$ *dependence of the flux. Thickness-map (middle, left), An-map (middle, right), MSE-map (bottom, right) Result of the selected (1 elementary point) expanded beam mapping SE measurement: MSE=0.059, Thickness=326.6 ± 8 nm, An=1.80 ± 0.03, Bn=-0.003 ± 0.0047, Cn=0.007 ± 0.0007, Ak=0.017 ± 0.007, Bk=1.44 ± 0.6 (bottom, left)*

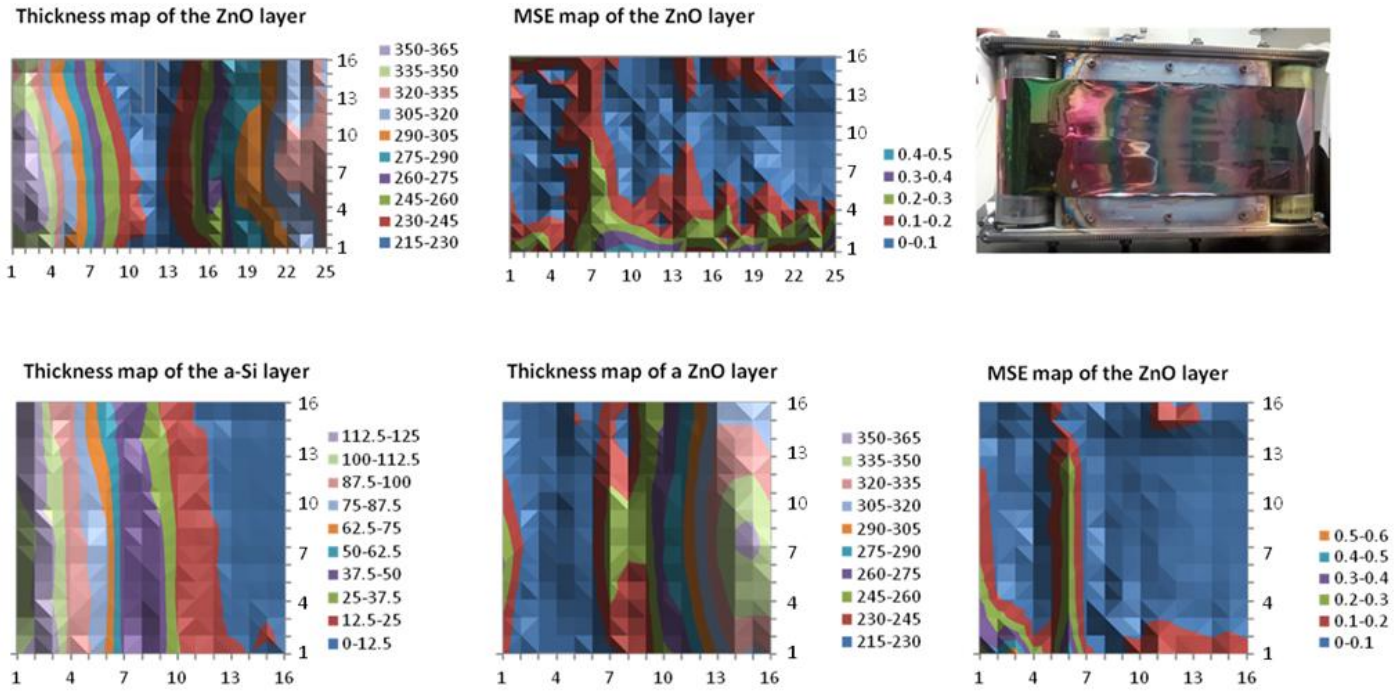

Figure 13

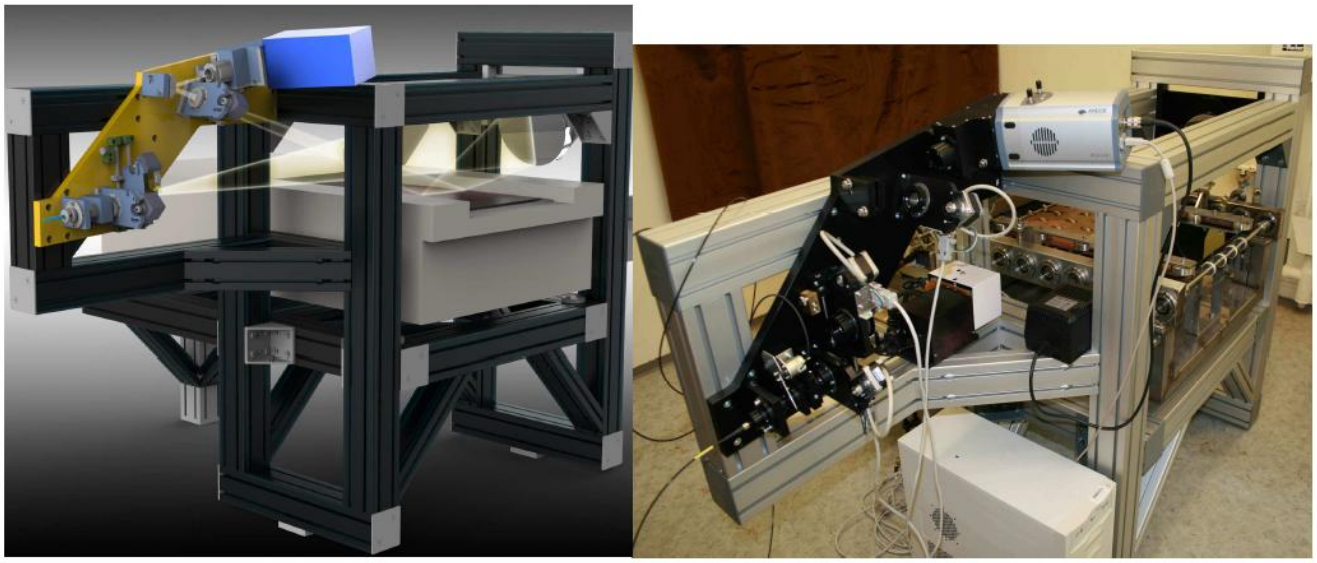

Figure 14 *Single-spectrum (350-1000 nm), rotating compensator expanded beam SE mapping device for 30-cm sample-size is completed at MFA (Budapest, Hungary); CAD-drawing with the beam-path (left) and photograph (right)*

Highlights

> Instrumentation developed provides a line image of spectroscopic ellipsometry data.

> The expanded-beam system (spectroscopic ellipsometry line imager) can measure in < 2 min.

> Expanded-beam ellipsometry system can monitor uniformity photovoltaic production lines

> Instrumentation for roll-to-roll or rigid plate substrates production lines.